Transition to turbulent thermal convection beyond Ra=10^{10} detected in numerical simulations

Alain P. Vincent,[1,2] and David A. Yuen,[3]
[1]*Département de Physique, Université de Montréal, CP 6128, Succ. Centre-Ville, Montréal, Québec, Canada H3C 3J7*
[2]*CERCA, 5160 Boulevard Décarie, Bureau 400, Montréal (Québec), Canada H3X 2H9*
[3]*Minnesota Supercomputer Institute and Department of Geology and Geophysics, University of Minnesota, Minneapolis, Minnesota 55415-1227*
(Received 25 August 1999)

We have conducted high-resolution two-dimensional calculations for a Boussinesq convection model with a Prandtl number of unity in an aspect-ratio 3 box, going from Rayleigh numbers between 10^8 to 10^{14}. A grid of 1024×3076 grid points consisting of a cosine-sine basis set has been employed for free-slip boundary conditions. We have found evidence for a transition involving the branching of plumes at a Rayleigh number of 10^{10}. Inside the core of these ''superplumes,'' the structure is extremely complex. There may be another transition at Ra of 10^{12}, where a secondary instability may develop in regions of the local Rayleigh number which becomes supercritical inside the core of the complex ''superplumes.'' For Ra of 10^8 to 10^{10}, Ra follows a $\frac{1}{3}$ power law in the Nusselt-Rayleigh number relationship. From Ra of 10^{10} to 10^{12}, Ra follows a $\frac{1}{2}$ power law. Above this value the Nusselt number becomes insensitive to the variation in the global Rayleigh number and this is due to the development of small-scale convection cells vertically aligned in the interior of the extremely high Ra number flow. The global Reynolds number scales as $\mathrm{Re}\approx\mathrm{Ra}^{1/4}$ up to Ra of 10^{14}. Scaling relationships based on global properties would not work in extremely high Ra situations beyond Ra of 10^{12} because of the complex turbulent layered convection in the core of the flow and the severe degradation of the boundary layers.

PACS number(s): 05.60.−k, 47.27.Te

I. INTRODUCTION

The idea that Rayleigh-Benard convection may become turbulent at a high enough Rayleigh number is very old [1–3]. Discrete transitions of convection on its route to turbulence had been predicted by Malkus [4] long ago. Laboratory experiments of helium gas under low temperature conditions have revealed that a new fully turbulent regime, beyond that of the hard-turbulent regime [5], may begin at $\mathrm{Ra}\approx10^{10}$ [6] with a theoretical Nu(Ra) relationship of $\mathrm{Nu}\approx\mathrm{Ra}^{1/2}$ [3]. This transition is found to occur in mercury for $\mathrm{Ra}\approx10^9$ [7]. The Reynolds number of the flow keeps on increasing with Ra [8]. The local Reynolds number in the boundary layer reaches a value characteristic of turbulence in the sense of Kolmogorov [9] and the heat transport is no longer dominated by conduction alone in the boundary layer but also by turbulent advection. A theory for plume population based on kinetics [10] for three-dimensional (3D) convection predicts a balance between the creation of plumes by boundary-layer instability and their disappearance by coalescing with other plumes. Such kinds of plume-plume collision at high Rayleigh number have been observed experimentally [11]. At low Rayleigh number plume merging is also an important process [12]. In the atmosphere, where the Rayleigh number is extremely high, plumes appear as the vertical motion of a swarm of warm bubbles. In dry isentropic vertically stratified media, such bubbles have been observed to be highly unstable, giving rise to a batch of secondary instabilities [13]. Another important distinction in high Rayleigh number convection is the existence of the large-scale flow with its associated shear. This idea has been postulated for high-Rayleigh-number convection [14] and is observed in most laboratory experiments (e.g., Ref. [15]). It is postulated to be at the heart of the $\mathrm{Nu}\approx\mathrm{Ra}^{2/7}$ scaling law [16]. The presence of a shear flow near the boundary layer would not change much of the heat flux [17] but in the case of a forced recirculating flow near the boundary, the heat flux was enhanced [18]. However, in numerical simulations with periodic boundary conditions, no large-scale flow was observed [19,20].

In the laboratory with no-slip boundary conditions, the thickness of the viscous boundary layer is found to decrease faster than the thickness of the thermal boundary layer with increasing Ra. The crossover point is expected to occur at around $\mathrm{Ra}\approx10^{15}$ [15], giving rise to the ''turbulent Kraichnan'' regime, where a significant part of the heat flux inside the boundary layer is now transported mainly by turbulence and only a small portion by conduction. In this regime, the predicted laws are $\mathrm{Nu}\approx\mathrm{Ra}^{1/2}$ and $\mathrm{Re}\approx\mathrm{Ra}^{1/2}$ [3,7]. In order to shed more light on this expected transition, we report in this paper direct numerical simulations of 2D Rayleigh-Benard convection with free-slip boundary conditions for Rayleigh numbers ranging from 10^8 to 10^{14}. We feel that only by reducing this high Ra problem to 2D are we able to make a big leap in the Rayleigh number space to be able to observe novel physical changes occurring in the turbulent regime. To make an equivalent leap in the direction of 3D high Rayleigh number convection would surely mean a postponement well into the first decade of the new millennium.

II. NUMERICAL MODEL AND ALGORITHM

The dimensionless equations describing finite Prandtl number convection with constant physical properties in the Boussinesq approximation are

$$\nabla\cdot\mathbf{V}=0, \tag{1}$$

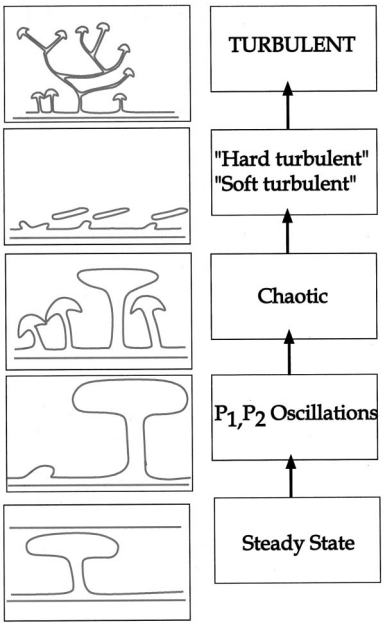

FIG. 1. Schematic drawing showing the development in the style of plumes ranging from steady-state plumes for low Rayleigh number $O(10^5)$ to the turbulent regime where branching of plumes take place at global Ra greater than 10^{10}.

$$\frac{\partial \mathbf{V}}{\partial t} + \boldsymbol{\nabla} \cdot (\mathbf{V}\mathbf{V}) = \mathrm{Pr}\Delta \mathbf{V} - \nabla P + \mathrm{Pr}\theta \mathbf{e_z} \tag{2}$$

$$\frac{\partial \theta}{\partial t} + \boldsymbol{\nabla} \cdot (\mathbf{V}\theta) = \Delta \theta + \mathrm{Ra} V_z \mathbf{e_z}, \tag{3}$$

where t is the dimensionless time based on thermal diffusion, θ is the deviation of the temperature T from the linear conductive profile ($T = T_{\mathrm{cond}} + \theta$), $\mathbf{V}$ is the velocity, and $\mathbf{e_z}$ is the vertical unit vector directed from the top to the bottom of the fluid layer. Ra is the thermal Rayleigh number for a base-heated configuration. A Prandtl number Pr of unity, characteristic of air, has been assumed. We have used the following scaling scheme in presenting the results: the layer thickness, the thermal diffusive time and for the temperature difference across the layer divided by the Rayleigh number. At very high Rayleigh numbers above 10^{10}, non-Boussinesq effects in thermal convection in air may be possible (e.g., Ref. [21]).

The numerical method employed has already been described in a previous work [22]. Basically this consists of a series of cosine and sine expansion, which satisfies naturally the top and bottom free-slip boundary conditions. Time-marching is accomplished by a mixed leap frog–Cranck-Nicholson two-step pressure correction scheme. A high-precision accuracy in the computer word length, at least 64 bits long, is needed for these high Rayleigh number simulations, where the time steps must be very small.

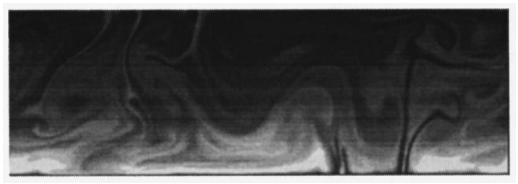

FIG. 2. Snapshot of the temperature deviation taken from the $\mathrm{Ra} = 10^8$ simulation of Vincent and Yuen (1999).

III. RESULTS

Plumes, which are hot upwellings developed in thermal convection, change their style and morphology with increasing Rayleigh number. We summarize the various stages of plume development with Ra by a schematic sketch, depicting the different transitions of plume structures from steady-state features at low Ra of around 10^5 to the P_1 and P_2 transitions [23], the chaotic regime [24], the soft and hard turbulent regime, which is marked by shear flow in the boundary layer and disconnected plumes [25,5,26] and finally to the turbulent regime and the phenomenon of plume branching, which lies at the heart of this paper (Fig. 1). Rayleigh-Benard convection in air up to $\mathrm{Ra} \approx 10^7$ has been studied in many numerical experiments [19,20,27]. Laboratory experiments have also been conducted at these Rayleigh numbers [7,6]. We [22] have investigated numerically the development of waves in thermal convection at $\mathrm{Ra} = 10^8$. A snapshot of the plume at this Ra is shown in Fig. 2. In Fig. 3 we show the flow at $\mathrm{Ra} = 10^{10}$. We have used as the initial condition the

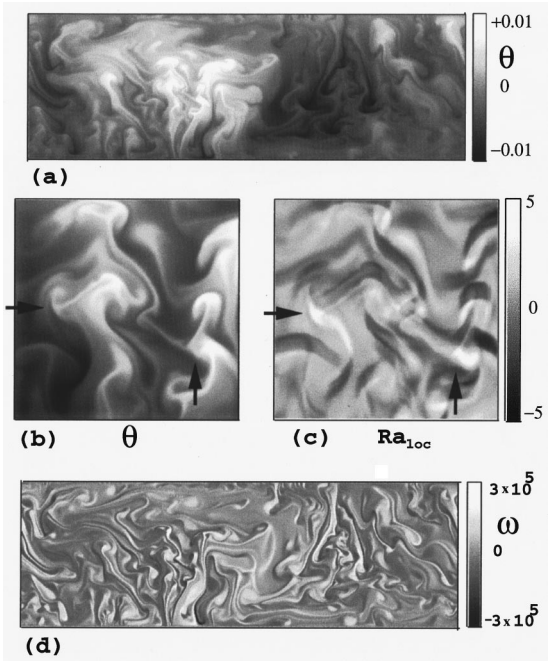

FIG. 3. Transition to turbulent convection. Sizes of the box are $L_x = 3$ $L_z = 1$. The global Rayleigh number is $\mathrm{Ra} = 10^{10}$ and the Prandtl number is $\mathrm{Pr} = 1$. The numerical resolution is $N_x = 1536$, $N_z = 512$ grid points. (a) Convective temperature field. Two superplumes or ''turbulent plumes'' are governing the flow. One ascending (left) and one descending (right). (b) Zoom of the center region of the ascending ''turbulent plume.'' Small plumes appear near the core of the flow as a result of a complex mechanism including the severing of a plume by a vortex collision and the further lift of the remaining plume patches by buoyancy and turbulent advection. At $\mathrm{Ra} = 10^{10}$, there is a balance between turbulence and buoyancy. (c) Local Rayleigh number distribution $\mathrm{Ra}(x,z)$. Plume creation inside the convective core is possible at two places [see arrows in (b) and (c)] where Ra is supercritical. (d) Transverse vorticity ω corresponding to Fig. 1(a).

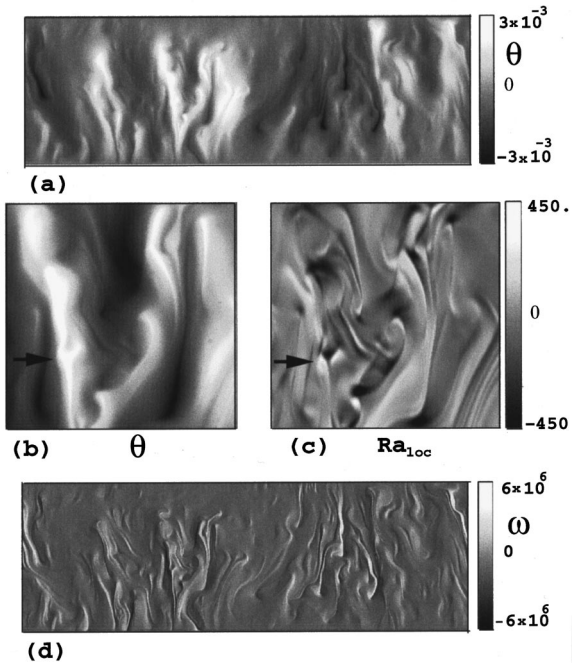

FIG. 4. Turbulent convection. Prandtl regime. $\mathrm{Ra}=10^{14}$. The numerical resolution is $N_x=3072$ $N_z=1024$ grid points. (a) Convective temperature field. Two superplumes or ''turbulent plumes'' are still governing the flow. At $\mathrm{Ra}=10^{14}$, buoyancy in the turbulent interior dominates again. (b) Zoom of the center region of the ascending ''Turbulent plume.'' (c) The spatial distribution of the local Rayleigh number corresponding to Fig. 2(b). Local Rayleigh number is calculated on the basis of the local temperature gradient surrounding a given grid point. Due to the very high Rayleigh number, the plumes reaches a critical local Rayleigh and smaller plumes are generated inside the core of the global flow [see arrows in (b) and (c)]. (d) Transverse vorticity ω distribution corresponding to Fig. 2(a).

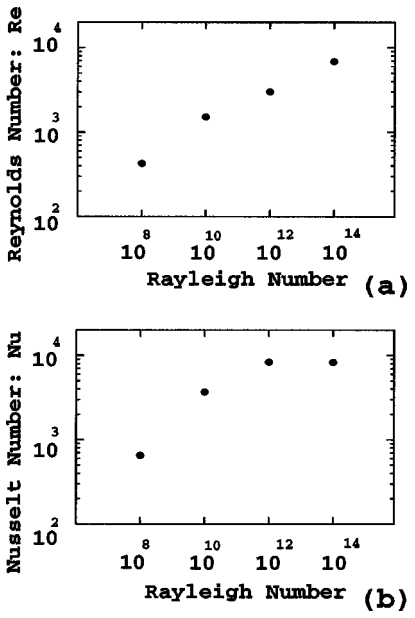

FIG. 5. (a) Turbulent Reynolds number versus global Rayleigh number. The scaling law is approximately $\mathrm{Re}\approx\mathrm{Ra}^{1/4}$. (b) Nusselt number versus global Rayleigh number. The transition is detected at $\mathrm{Ra}=10^{10}$. Below this value, we have $\mathrm{Nu}\approx\mathrm{Ra}^{1/3}$. Above $\mathrm{Ra}\approx10^{10}$ is the turbulent regime. In free-slip convection, there are no viscous boundary layers but the whole layer including the core of the flow may become turbulent. A part of the heat flux is now transported by turbulent diffusion. The scaling law is now $\mathrm{Nu}\approx\mathrm{Ra}^{1/2}$. Above $\mathrm{Ra}\approx10^{12}$, the Nusselt number does not change too much. Due to the very high Rayleigh number, the plumes reach a critical local Rayleigh and smaller plumes are generated inside the core [Fig. 2(c)]. This results in a temporary break of the vertical heat flux. The Nusselt number remains almost constant, while the Rayleigh number is increased. This transition is equivalent to an endothermic phase transition, occuring in the turbulent interior of the flow.

solution taken at the well-developed convective regime for $\mathrm{Ra}=10^8$ [22] in order to save computer time. The numerical solution is obtained by 512 points in the vertical and 1536 grid points along the horizontal direction in an aspect-ratio three box.

The temperature fluctuation is plotted in Fig. 3(a). Two packs of plumes are present in this flow. Hot material is ascending on the left of the box, while the right part of the box is filled with descending patches of cold fluid. Similar ''superplumes'' have been postulated by theorists in the convective envelopes inside stars [28]. Swarms of plumes branching from a single plume have been observed in non-Newtonian mantle convection [29]. We have observed that they are not always present but appear intermittently. For instance, the superplume we are discussing has survived a few overturn times and only after about 60 overturn-times is it destroyed. A zoom near the center of the ascending superplume is shown in Fig. 3(b) and reveals the complicated nature of the core. The Reynolds number is here above $\mathrm{Re}=1000$ and the flow is now turbulent. The corresponding local Rayleigh number distribution $\mathrm{Ra}(x,z)$ is shown in Fig. 3(c). The stripes associated with the plumehead are very close to sites with the highest local Ra and, in fact, are the new internal thermal boundary layers developed in high Ra convection. The plumes are broken and collide under the inertial forces (see the vortices). The corresponding vorticity field is displayed in Fig. 3(d). Thermal plumes are strongly related to the concentration of vorticity [30].

Next we increase the Rayleigh number up to 10^{14} by way of an intermediate stop at $\mathrm{Ra}=10^{12}$. The numerical resolution becomes now $N_z=1024\times N_x=3076$ grid points. Such a high resolution will soon become common within the capacity of powerful personal computers where a shared memory of a few gigabytes is the standard. The results are shown in Fig. 4. Displaying such a high resolution overwhelms the present-day monitor, but will not be the case soon when affordable high-resolution, high-content screens (e.g., IBM Roentgen) with 5 million pixels will soon appear in the market. In Fig. 4(a), are shown the temperature fluctuations and for comparison with the $\mathrm{Ra}=10^{10}$ case, the vorticity field is shown at the bottom in Fig. 4(d). As in the previous case, the two superplumes are still governing the flow. A zoom of the superplume thermal field is displayed in Fig. 4(b). We can observe the riverlike branching. Although the Reynolds number increases to a few thousands, buoyancy strongly dominates the flow. The local Rayleigh number may become supercritical for the instability to occur in some very restricted areas [see arrows in Fig. 4(c)] where the local tem-

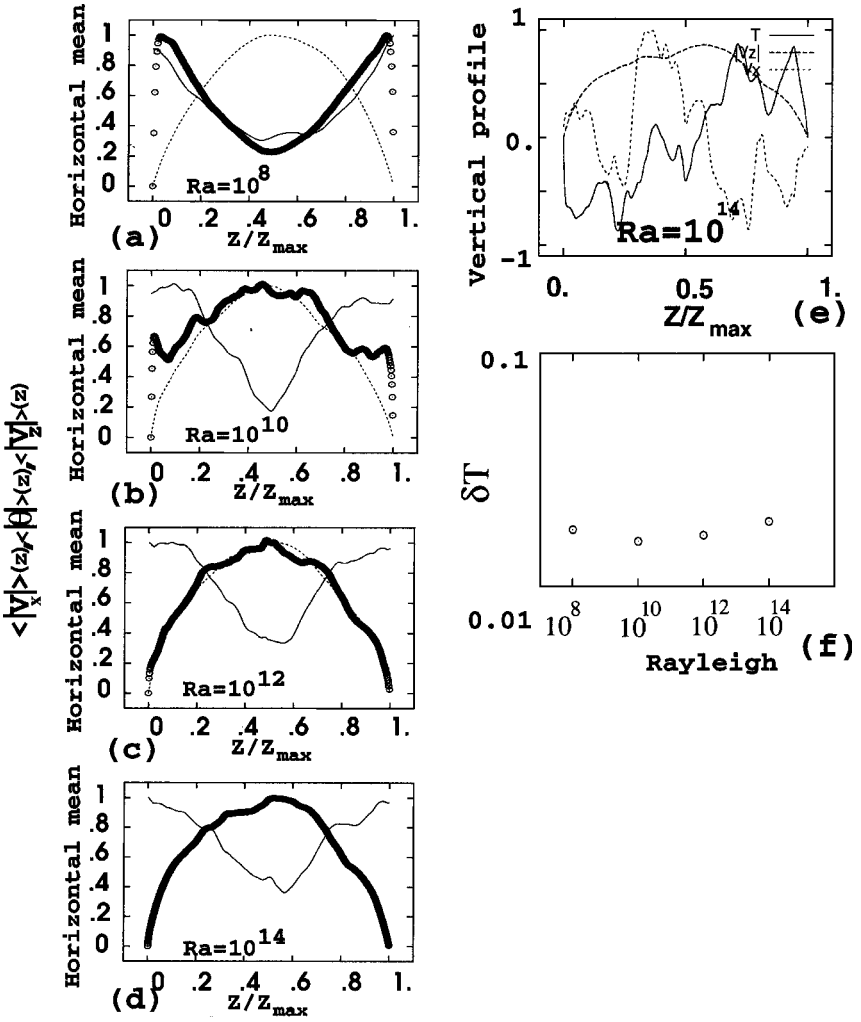

FIG. 6. Normalized temperature and velocity profiles inside the layer. Absolute value of temperature fluctuation profile $\langle|\theta|\rangle$ (open circles) and velocity profiles $\langle|V_x|\rangle$ (short dashed), $\langle|V_z|\rangle$ (long dashed) are plotted simultaneously. The Rayleigh number is increased from Ra $=10^8$ to Ra$=10^{14}$. Transition occurs at Ra$\approx 10^{10}$. (a) Ra$=10^8$. $\langle|V_x|\rangle$ and $\langle|\theta|\rangle$ have minima in the turbulent core and maxima in the boundary layers. It is the reverse for $\langle|V_z|\rangle$. (b) Ra$=10^{10}$. $\langle|\theta|\rangle$ is reversing and start to align with $\langle|V_z|\rangle$. (c) Ra$=10^{12}$. (d) Ra$=10^{14}$. Now $\langle|\theta|\rangle$ has exactly the same profile as $\langle|V_z|\rangle$. $\langle|\theta|\rangle$ and $\langle|V_z|\rangle$ have now maxima inside the turbulent core and minima near the boundary layers. The buoyancy in the core of the turbulent flow dominates the flow. (e) Normalized temperature and velocity profiles inside the layer $\langle\theta\rangle$, $\langle V_x\rangle$, $\langle|V_z|\rangle$ are plotted simultaneously showing the thermal boundary layers. The Rayleigh number is Ra$=10^{14}$. (f) Measured thickness δT of the thermal boundary layer versus the Rayleigh number. Above Ra$=10^{10}$, δT does not change.

perature gradients are strong enough. Experiments are underway to verify that in such a case, smaller plumes are locally generated. Such a physical phenomenon has been already observed in the atmosphere [13]. In this event, most of the heat flux would be temporarily broken up in the core of the cell and the global Nusselt number would become stationary with increasing Ra.

In Fig. 5(a) we plot the turbulent Reynolds number as monotically increasing with Ra from 10^8 upwards. We find Ra to be proportional to $\mathrm{Ra}^{1/4}$. The characteristic velocity for single plumes in the convective interior is still the free-fall velocity but the rms velocity behaves similar to the square root of the free-fall velocity. Turbulence moves plumes randomly as in a Levy flight (random walk). The trend of the Nusselt (Nu) versus the Rayleigh number holds much interest for the characterization of hard-turbulent convection (e.g., Ref. [16]), where the Nu, is found to be $\mathrm{Ra}^{2/7}$ for Ra up to 10^8. We have found that from Ra$=10^8$ to Ra$=10^{10}$, the Priestley ''$\frac{1}{3}$'' scaling law [2] of Nu$\approx\mathrm{Ra}^{1/3}$ holds. Both experimental [31,32] and theoretical [33] works on air and water have suggested the Nu$\approx\mathrm{Ra}^{1/3}$ in the turbulent regime beyond Ra$\approx 10^9$. From Ra$=10^{10}$ to Ra$=10^{12}$ we find the ''turbulent'' regime Nu$\approx\mathrm{Ra}^{1/2}$ [3]. Above this value, the Nusselt number does not change much with Ra for the reasons already discussed in Fig. 4. This asymptotic relationship for Ra$>10^{12}$ is displayed in Fig. 5(b). This hydrodynamic transition is analogous to an endothermic phase change taking place globally in a turbulent interior.

In Fig. 6 we focus on another aspect of the Ra$=10^{10}$ transition mechanism by looking at the horizontally averaged temperature and velocity profiles. At Ra$=10^8$, in Fig. 6(a) are plotted together the absolute values of normalized temperature fluctuations profile $|\theta(z)|$ and the two horizontally averaged [horizontal $|V_x(z)|$ and vertical $|V_z(z)|$] velocity profiles (absolute values). $|\theta(z)|$ is hot in the vicinity of the top and bottom boundaries and rather cold in the center of the box. The horizontal velocity has the same behavior. On the average, the velocity is strong near the boundaries and

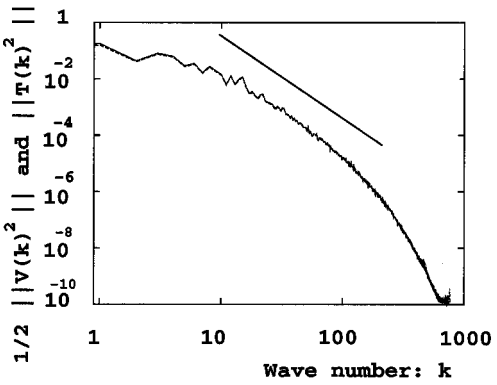

FIG. 7. Comparative spectra of thermal variance (– – –) and kinetic energy (---) at Ra$=10^{14}$. The slope is k^{-3}, thus reflecting two-dimensional turbulence and the tracerlike behavior of the temperature fluctuations.

weak in the core of the flow. With the free-slip boundary conditions, there are no viscous sublayer but with the two superplumes configuration, we have a large-scale flow in half of the box. The $|V_z(z)|$ profile shows that the vertical velocity is maximal near the turbulent core. At Ra$=10^{10}$ [Fig. 6(b)], the situation is the same except that the temperature profile starts to reverse. Somewhere, slightly below Ra $=10^{10}$ the cell would be almost entirely isothermal. In Fig. 6(c) we observe the transition continuing for Ra$=10^{12}$. The transition is finally achieved at Ra$=10^{14}$ where the temperature profile matches almost exactly the vertical velocity profile [Fig. 4(c)]. Over the entire domain and on the average, the buoyancy in this regime governs the flow. The above results are not obvious when the absolute value is not taken. Typical velocity and temperature fluctuation profiles are shown in Fig. 6(e). The $\langle\theta\rangle$ (z) profile shows very thin boundary layers but also internal sublayers and the $\langle V_x\rangle$ (z) profile, as expected, does not show viscous boundary layer. As the Rayleigh number is increased, the thickness of the thermal boundary layer stays almost constant [Fig. 6(f)].

The high Reynolds number flow imposes a two-dimensional turbulence and hence a k^{-3} scaling law (e.g., Ref. [34] for both the kinetic energy and the temperature fluctuations over about a decade in wave number). We display this k^{-3} dependence in Fig. 7 for Ra$=10^{14}$. Most of the numerical resolution at this high Ra is used apparently for delineating the dissipative range.

In Fig. 8 we show, the horizontally averaged vertical temperature gradient $\langle dT/dz\rangle$, where the brackets indicate an horizontal average, for Ra ranging from 10^8 to 10^{14}. As in Fig. 6, we observe a transition in the pattern of the $\langle dT/dz\rangle$ profile at Ra of 10^{10}. At Ra$=10^{14}$, there are many steps in $\langle dT/dz\rangle$ indicative of the prevalence of turbulent small-scale layered convection, which can be observed in the thermal contours of the superplumes shown in Figs. 3 and 4.

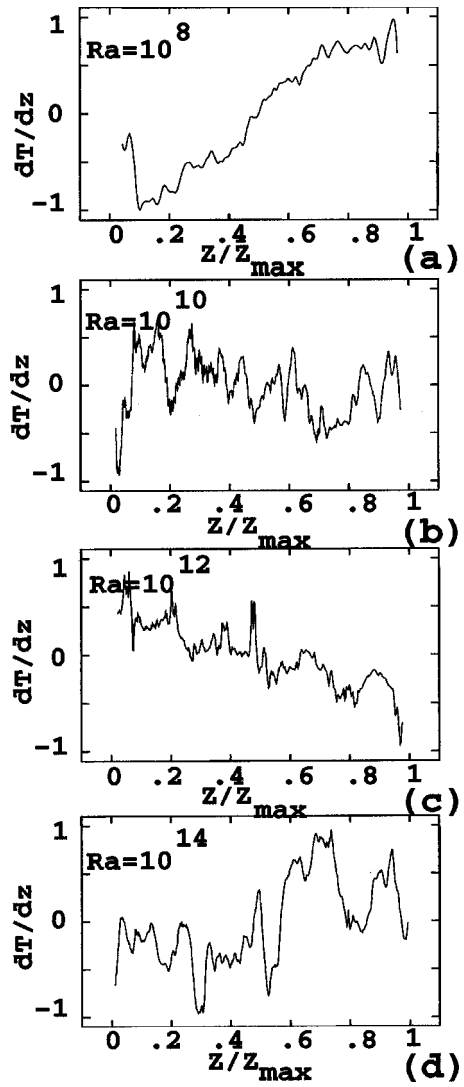

FIG. 8. The vertical profile of the horizontally averaged vertical temperature gradient with varying Rayleigh numbers. (a) Ra $=10^8$. (b) Ra$=10^{10}$. (c) Ra$=10^{12}$. (d) Ra$=10^{14}$. For Ra of 10^{12} to 10^{14}, we can see signs of layered convection by the series of steps in the profile.

IV. CONCLUSION AND OPEN QUESTIONS

In this paper we have shown for the first time, a picture of a ''superplume'' which may contribute a significant part of the heat flux in convective envelopes inside stars [28]. This shows that it is now possible and necessary to test and use the large-eddy simulation technique [35] in convection because we have enough resolution from DNS solutions. Recent work on finite Prandtl number convection by LES [8] is encouraging for Ra up to 10^{10}. Extending such a study to Ra of 10^{14} still requires a nontrivial amount of effort in terms of computational work and would be even more difficult in three dimensions.

As with the free-slip boundary conditions, we have found that there exist no viscous sublayers for these high Rayleigh numbers. Therefore, the mechanism leading to the scaling laws in the turbulent regime remains still an open issue.

We have observed that a transition occurs at Ra$\approx 10^{10}$ where the (inertial) two-dimensional turbulence governs the flow and that another transition occurs apparently at Ra $\approx 10^{12}$. At these Rayleigh numbers the buoyancy is again the dominating driving force and the vertical velocity is aligned with the temperature fluctuations. The local Rayleigh number, which can be measured by the local temperature gradient, becomes supercritical in some areas and it is now an open question to determine whether such a condition would

give rise to secondary convective instabilities in the interior.

If this proves to be the case, then we may explain why the Nusselt number does not increase further when the Rayleigh number is increased between $Ra \approx 10^{12}$ and $Ra \approx 10^{14}$. These results concerning Nu(Ra) for $Ra > 10^{12}$, if valid, have strong implications on the thermal evolution inside Jovian moons, such as Europa, whose Ra is very high [$Ra \approx O(10^{17})$] because of a deep ocean of water [36]. Our 2D results will surely require verification from 3D simulations, but this would follow suit in a long time.

ACKNOWLEDGMENTS

We thank Professor S. Balachandar for a conscientious review. This research has been supported by the DMS division of NSF (Grant No. NSF-DMS 96-22889) and the geophysics program of the NSF. These simulations were conducted at Minnesota Supercomputer Institute on the IBM/SP2 cluster system. Our code is a modified version of a public domain code originally written by Anil Deane for double-diffusive convection.

[1] L. Prandtl, Beitr. Phys. Atmos. **19**, 188 (1932).
[2] C. H. B. Priestley, Aust. J. Phys. **7**, 176 (1954).
[3] R. H. Kraichnan, Phys. Fluids **5**, 1374 (1962).
[4] W. V. R. Malkus, Proc. R. Soc. London Ser. A **225**, 185 (1954).
[5] B. Castaing, G. Gunaratne, F. Heslot, L. Kadanoff, A. Libchaber, S. Thomae, X. Zh. Wu, S. Zaleski, and G. Zanetti, J. Fluid Mech. **204**, 1 (1989).
[6] X. Chavanne, F. Chillà, B. Castaing, B. Hébral, B. Chabaud, and J. Chaussy, Phys. Rev. Lett. **79**, 3648 (1997).
[7] S. Cioni, S. Ciliberto, and J. Sommeria, J. Fluid Mech. **335**, 111 (1997).
[8] N. Cantin, A. P. Vincent, and D. A. Yuen, Geophys. J. Int. **140**, 1 (2000); **140**, 163 (2000).
[9] U. Frisch, *Turbulence: The Legacy of A. N. Kolmogorov* (Cambridge University Press, Cambridge, 1995).
[10] E. M. Parmentier and C. Sotin, Phys. Fluids **12**, 609 (2000).
[11] E. Moses, G. Zocchi, and A. Libchaber, J. Fluid Mech. **251**, 581 (1993).
[12] A. P. Vincent and D. A. Yuen, Phys. Rev. A **38**, 1 (1988); **38**, 328 (1988).
[13] A. Robert, J. Atmos. Sci. **50**, 1865 (1993).
[14] R. Krishnamurti and L. N. Howard, Proc. Natl. Acad. Sci. USA **78**, 1981 (1981).
[15] A. Belmonte, A. Tilgner, and A. Libchaber, Phys. Rev. E **50**, 269 (1994).
[16] E. D. Siggia, Annu. Rev. Fluid Mech. **26**, 137 (1994).
[17] S. Ciliberto, S. Cioni, and C. Laroche, Phys. Rev. E **54**, R5901 (1996).
[18] T. H. Solomon and J. P. Gollub, Phys. Rev. Lett. **64**, 2382 (1990).
[19] S. Balachandar, M. R. Maxey, and L. Sirovich, J. Sci. Comput. **4**, 219 (1989).
[20] R. M. Kerr, J. Fluid Mech. **310**, 139 (1996).
[21] X. Z. Wu and A. Libchaber, Phys. Rev. A **45**, 842 (1992).
[22] A. P. Vincent and D. A. Yuen, Phys. Rev. E **60**, 3 (1999); **60**, 2957 (1999).
[23] P. Bergé, Y. Pommeau, and C. Vidal, *L'ordre dans le Chaos* (Hermann, Paris, 1984).
[24] A. Libchaber, S. Fauve, and C. Laroche, Physica D **7**, 73 (1983).
[25] F. Heslot, B. Castaing, and A. Libchaber, Phys. Rev. A **36**, 5870 (1987).
[26] A. P. Vincent, U. Hansen, D. A. Yuen, A. V. Malevsky, and S. E. Langenberger, Phys. Fluids A **3**, 2222 (1991).
[27] J. Werne, Phys. Rev. E **49**, 5 (1994); **49**, 4072 (1994).
[28] M. Rieutord and J.-P. Zahn, Astron. Astrophys. **296**, 127 (1995).
[29] A. V. Malevsky, D. A. Yuen, and L. M. Weyer, Geophys. Res. Lett. **19**, 27 (1992).
[30] T. Cortese and S. Balachandar, Phys. Fluids **5**, 3226 (1993).
[31] R. J. Goldstein and T. Y. Chu, Prog. Heat Mass Transfer **2**, 55 (1971).
[32] R. J. Goldstein and S. Tokuda, Int. J. Heat Mass Transf. **23**, 738 (1980).
[33] R. R. Long, J. Fluid Mech. **73**, 445 (1976).
[34] M. Lesieur, *Turbulence in Fluids*, 3rd ed. (Kluwer Academic Publisher, Dordrecht, 1997).
[35] J. H. Ferziger, in *Numerical methods in Fluid Mechanics*, edited by A. Vincent, Vol. 16 of CRM Proceedings Lecture Notes (American Mathematical Society, Providence, RI, 1998).
[36] M. H. Carr, M. H. Belton, and C. R. Chapman, Nature (London) **391**, 363 (1998).